ECBC-TR-XXX

TEMPORAL-SPECTRAL DETECTION IN LONG WAVE INFRARED HYPERSPECTRAL IMAGERY

Daniel C. Heinz
Charles E. Davidson
Avishai Ben-David

Science and Technology Corp.
500 Edgewood Rd, Suite 205,
Edgewood MD 21040,
410 436-7736

Edgewood Chemical Biological Center,Aberdeen Proving Ground, MD 21010,
410 436-6631

June 2008

Report Documentation Page

Form Approved
OMB No. 0704-0188

1. REPORT DATE	2. REPORT TYPE	3. DATES COVERED
JUN 2008		**00-00-2008 to 00-00-2008**

4. TITLE AND SUBTITLE	5a. CONTRACT NUMBER
Temporal-Spectral Detection in Long Wave Infrared Hyperspectral Imagery	5b. GRANT NUMBER
	5c. PROGRAM ELEMENT NUMBER
6. AUTHOR(S)	5d. PROJECT NUMBER
	5e. TASK NUMBER
	5f. WORK UNIT NUMBER
7. PERFORMING ORGANIZATION NAME(S) AND ADDRESS(ES) **Science and Technology Corp,500 Edgewood Rd, Suite 205,Edgewood,MD,21040**	8. PERFORMING ORGANIZATION REPORT NUMBER
9. SPONSORING/MONITORING AGENCY NAME(S) AND ADDRESS(ES)	10. SPONSOR/MONITOR'S ACRONYM(S)
	11. SPONSOR/MONITOR'S REPORT NUMBER(S)

12. DISTRIBUTION/AVAILABILITY STATEMENT
Approved for public release; distribution unlimited

13. SUPPLEMENTARY NOTES

14. ABSTRACT

15. SUBJECT TERMS

16. SECURITY CLASSIFICATION OF:			17. LIMITATION OF ABSTRACT	18. NUMBER OF PAGES	19a. NAME OF RESPONSIBLE PERSON
a. REPORT **unclassified**	b. ABSTRACT **unclassified**	c. THIS PAGE **unclassified**	**Same as Report (SAR)**	**15**	

Disclaimer

The findings in this report are not to be construed as an official Department of the Army position unless so designated by other authorizing documents.

Report Documentation Page

TABLE OF CONTENTS

FIGURES

TABLES

ABSTRACT

Ground-based staring hyperspectral chemical detectors allow for repeated measurements through time with near-perfect image registration. The problem with standard spectral based hyperspectral detection algorithms is that they do not make effective use of this temporal information. In this paper we show that significant improvements in detection performance for staring geometry can be made by making use of statistical information obtained from previous samples and new temporal-spectral detection algorithms are developed. These new algorithms have the advantage that they limit detection to regions where both temporally and spectrally significant events have occurred. We discuss the development of these algorithms and demonstrate the performance of both temporal-spectral and spectral detectors for detection of gaseous plumes using data from the FIRST (Field-Portable Imaging Radiometric Spectrometer Technology) passive long wave infrared (LWIR) hyperspectral sensor.

INTRODUCTION

Hyperspectral imagery is often visualized as a three-dimensional image cube, where two of the dimensions are used to indicate spatial location of an image pixel and the third dimension specifies a spectral band. When the hyperspectral sensor is set-up to stare at a fixed location a fourth dimension of time is created as each new cube is sampled in time. Therefore, we are dealing with 'hyper' remote sensing where we have hyperspectral (many contiguous spectral bands), hyperspatial (many pixels at about 1m spacing) and hypertemporal (repeated coverage every few seconds) imagery [1]. In a ground-based stare-mode geometry each new cube will have almost perfect spatial registration with the previous data cubes.

There are three time scales inherent in a hyperspectral sensor monitoring for gaseous plumes: electronic noise on the MHz scale, atmospheric turbulence on the KHz scale, and long time scale (Hz) for atmospheric transmission drift [2, 3]. Since the hyperspectral sensor operates on the Hz scale the variance induced on the signal due to higher frequency (KHz and MHz) will be reduced via averaging due to the independence of samples. We will explore the amount of averaging required and how it relates to the third time scale.

It will be shown that by combining temporal and spectral information we are able to significantly increase the signal-to-noise ratio (SNR). This significant SNR increase allows the detection thresholds to be raised, which greatly reduces the false alarm rate.

TEMPORAL-SPECTRAL DETECTION ALGORITHMS

The temporal-spectral detection algorithms function to detect targets by using statistics from time t_1 to detect targets at time t_2. The algorithms are developed as follows. Let l represent the number of spectral bands and let $\mathbf{x}_{i,j,t_1}$ be an $l \times 1$ column pixel vector at spatial location (i, j) and at sample time t_1. To simplify the following notation the (i, j) spatial location information is omitted. In multivariate statistical analysis the Mahalanobis distance squared of a test pixel spectrum from the mean of the background class is given by

$$D_{AD} = \left(\mathbf{x}_{t_2} - \boldsymbol{\mu}_{t_0}\right)^T \mathbf{C}_{t_0}^{-1} \left(\mathbf{x}_{t_2} - \boldsymbol{\mu}_{t_0}\right) \tag{1}$$

and in the literature is known as an anomaly detector (AD) [4,5]. In Eq. 1 the mean, $\boldsymbol{\mu}_{t_0}$ and covariance, $\mathbf{C}_{t_0}$ are measured only once at a time t_0 when it is assumed that the target is not present in the scene. This method assumes that the mean and covariance are stationary. There are many ways to calculate the mean and covariance (e.g. image segmentation), in this paper we use the global mean and covariance.

By turning Eq. 1 into a ratio and making use of both past and present statistics we can form two temporal-spectral detectors. The first, referred to as the temporal-spectral anomaly detector (*TSAD*), is given as follows

$$D_{TSAD} = \frac{\left(\mathbf{x}_{t_2} - \boldsymbol{\mu}_{t_2}\right)^T \mathbf{C}_{t_1}^{-1}\left(\mathbf{x}_{t_2} - \boldsymbol{\mu}_{t_2}\right)}{\left(\mathbf{x}_{t_1} - \boldsymbol{\mu}_{t_1}\right)^T \mathbf{C}_{t_1}^{-1}\left(\mathbf{x}_{t_1} - \boldsymbol{\mu}_{t_1}\right)} \tag{2}$$

The second, referred to as the temporal-spectral covariance detector (*TSCD*), is given as follows

$$D_{TSCD} = \frac{\left(\mathbf{x}_{t_2} - \boldsymbol{\mu}_{t_2}\right)^T \mathbf{C}_{t_1}^{-1}\left(\mathbf{x}_{t_2} - \boldsymbol{\mu}_{t_2}\right)}{\left(\mathbf{x}_{t_2} - \boldsymbol{\mu}_{t_2}\right)^T \mathbf{C}_{t_2}^{-1}\left(\mathbf{x}_{t_2} - \boldsymbol{\mu}_{t_2}\right)} \tag{3}$$

Eqs. 2 and 3 are ratios of anomaly detectors. In order for the *TSAD* to improve detection performance the anomaly (e.g. gaseous plume) is assumed not to be present at pixel location (i, j) at time t_1 or at least that the concentration of target gas has increased from time t_1 to time t_2 at pixel location (i, j). Both the *TSAD* and *TSCD* assume that the covariance matrix formed at time t_1 is free from a temporal signal or when the gas concentration has increased from time t_1 to time t_2 to have less temporal signal than the covariance matrix formed at time t_2. The *TSAD* further assumes that the plume is either present in only a portion of the scene or non-uniform. Under these assumptions both the ratios in Eqs. 2 and 3 will be larger than one for any pixel vector $\mathbf{x}_{t_2}$ that contains an anomalous temporal signal. However, if the gas concentration is determined to be decreasing when the system is started then the ratios in both Eqs. 2 and 3 can be inverted in order to improve detection performance.

Eqs. 2 and 3 are easily coupled with any standard detector such as the matched filter (MF) or adaptive coherence/cosine estimator (ACE) detector [5]. The matched filter is given by Eq. 4

$$D_{MFt_0} = \frac{\left(\mathbf{x}_{t_2} - \boldsymbol{\mu}_{t_0}\right)^T \mathbf{C}_{t_o}^{-1}\mathbf{t}}{\mathbf{t}^T \mathbf{C}_{t_o}^{-1}\mathbf{t}}, \tag{4}$$

where $\mathbf{t}$ is the target vector of interest. Like the AD, the mean and covariance are measured only once at a time t_0. Again, this assumes that the mean and covariance are stationary. Another variation of the matched filter given by

$$D_{MFt_2} = \frac{\left(\mathbf{x}_{t_2} - \boldsymbol{\mu}_{t_2}\right)^T \mathbf{C}_{t_2}^{-1}\mathbf{t}}{\mathbf{t}^T \mathbf{C}_{t_2}^{-1}\mathbf{t}}, \tag{5}$$

uses data only at the present time. This method does not require the stationarity of Eq. 4, but its performance will be reduced by the presence of signal at time t_2 due to whitening. By incorporating the use of covariance matrix at time t_1 into Eq. 5 we get another version of the matched filter that uses the

covariance matrix formed at time t_1 when the scene is potentially free from target signal or has less target signal than the covariance matrix formed at time t_2

$$D_{MFt_1} = \frac{\left(\mathbf{x}_{t_2} - \boldsymbol{\mu}_{t_2}\right)^T \mathbf{C}_{t_1}^{-1}\mathbf{t}}{\mathbf{t}^T \mathbf{C}_{t_1}^{-1}\mathbf{t}}. \tag{6}$$

This method assumes stationarity over the short period from t_1 to t_2. By coupling the *TSAD* and/or *TSCD* detectors with the matched detector the following three temporal-spectral matched filter (*TSMF*) detectors are formed.

$$D_{TSMFAD} = D_{MFt_1} \times D_{TSAD} \tag{7}$$

$$D_{TSMFCD} = D_{MFt_1} \times D_{TSCD} \tag{8}$$

$$D_{TSMF} = D_{MFt_1} \times D_{TSAD} \times D_{TSCD} \tag{9}$$

The advantage of the last 3 detectors (Equations 7-9) is that they combine temporal knowledge with spectral knowledge. Therefore, they only alarm when a pixel vector contains both a temporally anomalous signal which is a good match spectrally with the target vector.

For the matched filter SNR performance can be characterized once the inverse covariance matrix is known. If we let

$$\mathbf{y}_0 \sim N(\mathbf{0}, \mathbf{C}) \tag{10}$$

$$\mathbf{y}_1 \sim N(\mathbf{t}, \mathbf{C}) \tag{11}$$

where $\mathbf{y}_0$ is the signal model under hypothesis H_0 and $\mathbf{y}_1$ signal model under hypothesis H_1, with $\mathbf{t}$ representing the target signal vector and $\mathbf{C}$ the covariance matrix. We can then whiten $\mathbf{y}_0$ and $\mathbf{y}_1$ by multiplying by $\mathbf{C}^{-\frac{1}{2}}$. If we let

$$\mathbf{z}_0 = \mathbf{C}^{-\frac{1}{2}}\mathbf{y}_o \tag{12}$$

$$\mathbf{z}_1 = \mathbf{C}^{-\frac{1}{2}}\mathbf{y}_1 \tag{13}$$

Then

$$\mathbf{z}_0 \sim N(\mathbf{0}, \mathbf{I}) \tag{14}$$

$$\mathbf{z}_1 \sim N(\mathbf{s}, \mathbf{I}) \tag{15}$$

where,

$$\mathbf{s} = \mathbf{C}^{-\frac{1}{2}}\mathbf{t} \tag{16}$$

The unnormalized matched filter is given by:

$$M = \mathbf{z}^T\mathbf{s} \tag{17}$$

then

$$M \sim \left\{ \frac{N\left(0, \mathbf{s}^t\mathbf{s}\right) \; under \; H_0}{N\left(\mathbf{s}^t\mathbf{s}, \mathbf{s}^t\mathbf{s}\right) \; under \; H_1} \right\} \tag{18}$$

SNR can be defined as the mean score under H_1 divided by the standard deviation of the score under H_0; therefore, SNR for the matched filter is simply

$$SNR = \sqrt{\mathbf{s}^t\mathbf{s}} \, . \tag{19}$$

EXPERIMENTAL RESULTS

The Data used in the following experiments are from FIRST hyperspectral sensor [6]. The data was collected in 2006 at Dugway, UT. Three FIRST sensors with focal plane array up to 256 x 320 were used to capture data. The sensors were setup to stare at a fixed location where the simulant would be released. Frames were captured approximately every 6 seconds. Visible imagery was collected using a co-aligned camera. Figure 1 shows the visible image with broadband IR overlay (150 x 320).

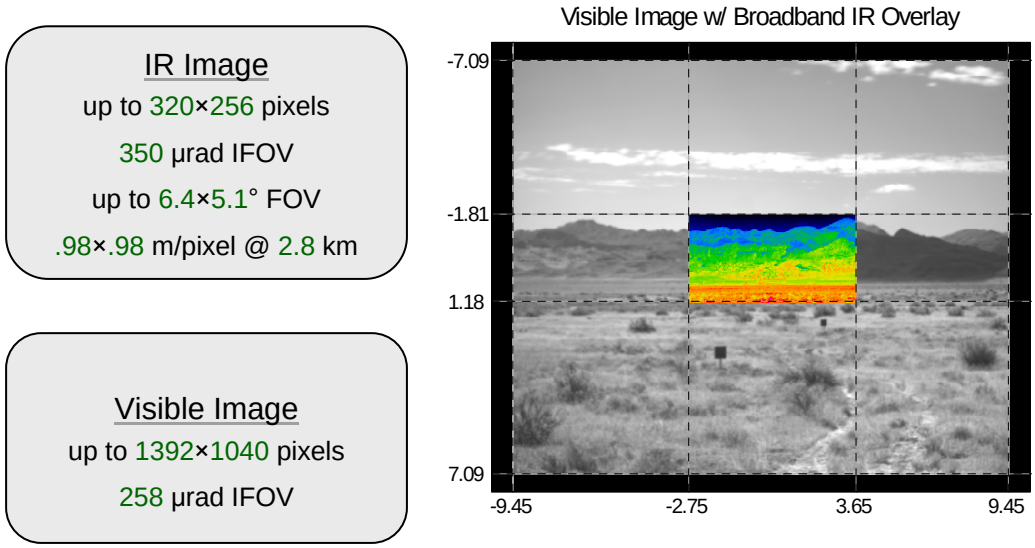

Figure 1. Visible image with broadband IR overlay (150x320) showing location of data acquisition.

Since there are 8 methods to compare (Equations 2-9) we started with only Equations 2-6. We began by examining the performance of each algorithm versus SNR. A simulation was conducted by inserting SF_6 from our library spectra into row 64 of a data cube free of target signal using half the focal plane array (128 x 320). The signal was set to have a SNR of approximately 45 (this corresponds to a concentration path length of approximately 135 mg/m^2 and delta temperature of 2 degrees) in column 1 of row 64 and linearly decay to 0 in column 320 of row 64. The signal to noise was calculated by taking the norm of the inserted SF_6 signal divided by the standard deviation of the noise measured at each pixel in row 64. The input SNR can be used as a measure for the matched filter performance; for instance, if the inverse covariance matrix is equal to the identity matrix then the matched filter SNR will be about equal to the measured input SNR (Eq. 19). However if the target vector is whitened by the inverse covariance matrix

then the matched filter performance will be poor. This is the main advantage of the temporal-spectral approach in which earlier covariance matrices without target are used to enhance SNR performance.

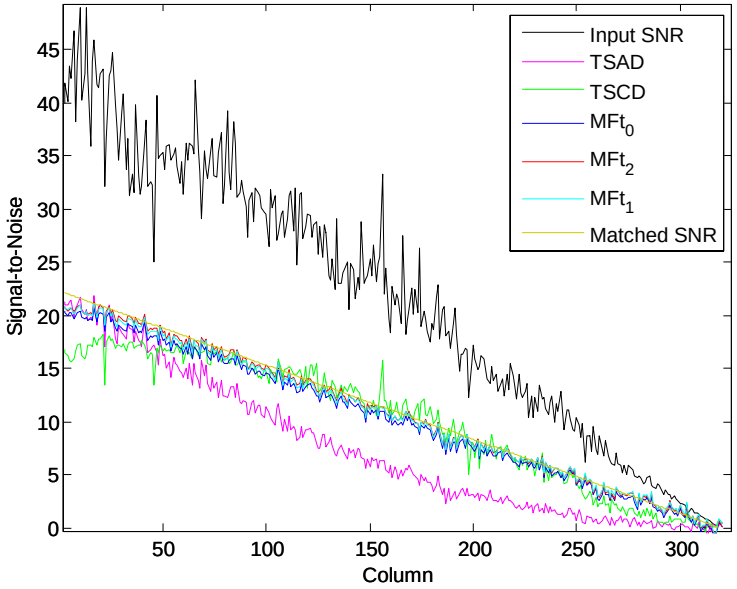

Figure 2. Detectors (Eqs. 2-6 & Eq. 19) SNR performance along the plume. The black line indicates the input SNR. The dark yellow line indicates predicted matched filter performance (Eq. 19) (Simulation).

Figure 2 contains a plot of the detectors (Eqs. 2-6 & Eq. 19) SNR performance where the noise was calculated by taking the standard deviation of all pixels except for those in row 64. The two matched filters MF_{t_1} and MF_{t_2} had almost identical performance. Their performance was mostly equal to the predicted matched filter SNR performance of Eq. 19. The matched filter, MF_{t_0} of Eq. 4 performed slightly worse than the other two matched filters since the data was not completely stationary. The *TSAD* (Eq. 2) had the worst performance of all the detectors at low SNR values, but did the best at higher SNR values. The *TSCD* (Eq. 3) performed similar to the matched filters.

The three additional detectors (Eqs. 7-9) were formed by coupling the *TSAD* and/or *TSCD* detectors with the matched detector. Figure 3 shows the results for these detectors using the same data and input signal as in Figure 2. As we can see, at the higher SNR values the *TSMF* performed extremely well. Figure 4 shows the region in Figure 3 from columns 160 to column 320. Comparing Figure 2 and 4 we see that performance the *TSMFAD* and *TSMF* of Figure 4 are closer to the input SNR than the matched filters of Figure 2 at low input SNR values and start to have a significant improvement in performance for input SNR values of 12 and greater.

In the following we analyze the performance of the detectors for field data with a release of SF_6 using library spectra as the target vector. In order to determine if frame averaging would help reduce the noise we examined the global mean over 100 frames of data without any target signal present. Window sizes from 1 to 7 frames over the 100 frame sequence where used to calculate the mean standard deviation of global mean. The mean standard deviation followed the expected square-root of the number of frames reduction for window size up to about 5 frames. Therefore, the mean is stationary for about five frames (30 seconds). This means that the atmospheric transmission drift on the Hz scale starts to become significant after about 30 seconds. In [1] it was shown that atmospheric drift was significant for periods as shorts as 5 seconds.

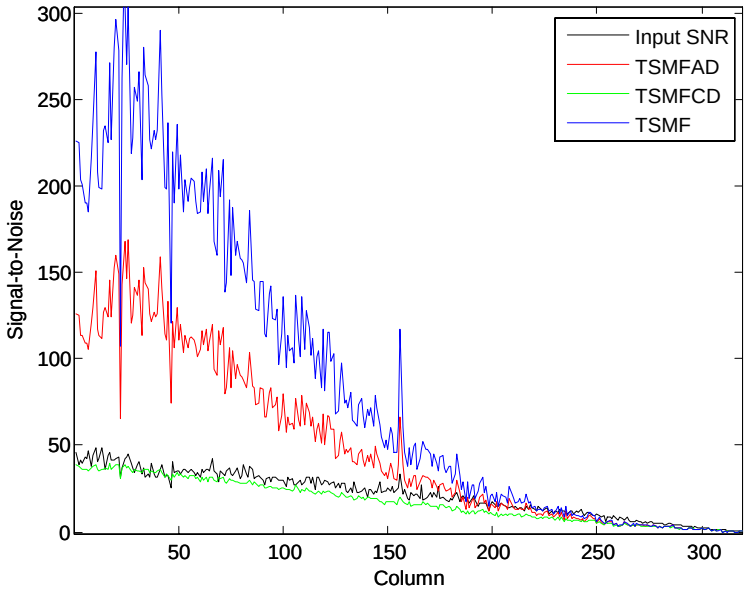

Figure 3. Detectors (Eqs. 7-9) SNR performance along the plume. The black line indicates the input SNR (Simulation).

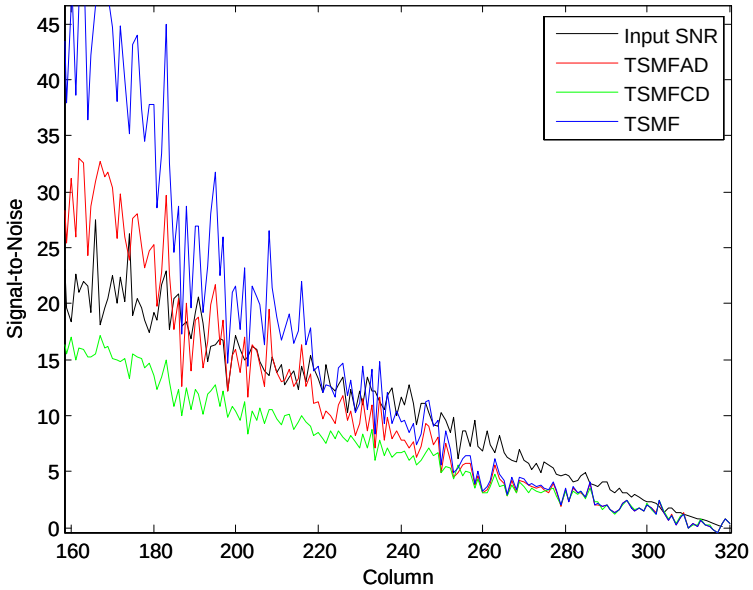

Figure 4. Portion of Figure 3 where SNR is lower (Simulation).

The second factor in determining how many frames to average is the signal. If the signal remains present in a pixel for multiple frames then it is beneficial to average and reduce the noise as stated above. The signal movement will be dependent on the size of the plume and the wind speed and direction. By examining the plume in the field data it was determined that the wind speed was approximately 2 m/s in a direction perpendicular to the sensor and the plume was about 72 meters across as viewed by the sensor and at a distance such that each pixel is 1m x 1m. Consequently, the plume will remain in a pixel for

about 36 seconds or six frames. However, the plume was not of uniform intensity with the brightest portion being near the center of the plume and the dimmest portion at the outer radii.

In order to determine if frame averaging is useful, a subset of the data, which contained signal with low SNR, consisting of rows 1 through 70 and columns 1 through 320 was used. The weak signal in row 65 was used to measure performance. Table I contains results for the SNR performance of the *TSMF* with from 1 to 5 frames of averaging.

Table 1. SNR Performance of Frame Averaging

Frames Averaged	SNR Performance
1	24.1
2	31.4
3	43.2
4	33.2
5	23.8

In this case, three frames of averaging had the best performance. Figure 5 contains results for Equations 2, 3, and 6-9 with the noise normalized to that of the *TSMF* detector using three frames of averaging for both t_1 and t_2.

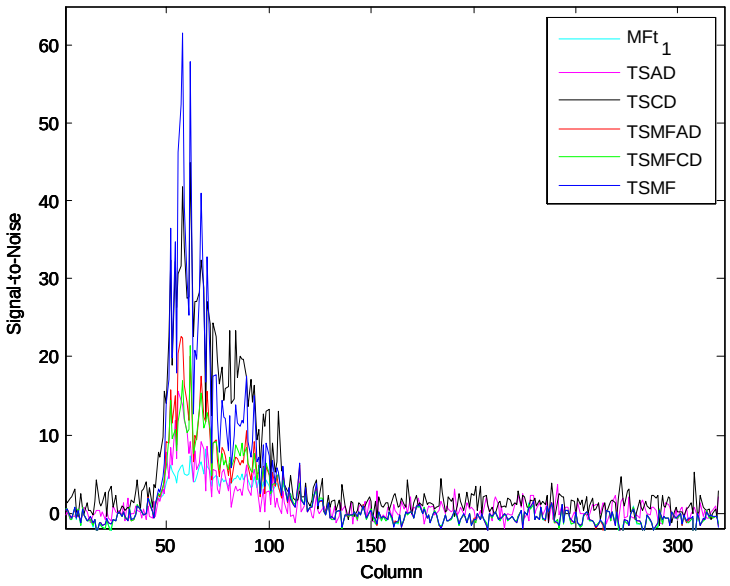

Figure 5. Performance of detectors on a release of SF_6 (Field Data).

As we can see, *TSMF* performed the best. *TSCD* performed second best, and performance of the *TSMFCD* was worse than *TSCD*. Based on these results we may want to create a temporal spectral detector by coupling Eqs. 2 and 3. However, Eqs. 2 and 3 are anomaly detectors and will alarm to any anomalous gaseous plume, but the matched filter will only alarm to target vector like plumes.

If the plume is present in a pixel for more than one frame we can improve performance further by cascading the detector outputs. For instance, if we repeat the experiment of Figure 5, but multiply the output of two consecutive detector outputs we get the results of Figure 6. This results in a significant SNR performance improvement. These high SNR values allow the detection thresholds to be raised which will result in a significant drop in false alarms. Even if the plume is not present in a single pixel during

two consecutive frames we could use a more sophisticated algorithm which searches the FOV to align the plume from one frame to the next, provided there is adequate SNR in each frame.

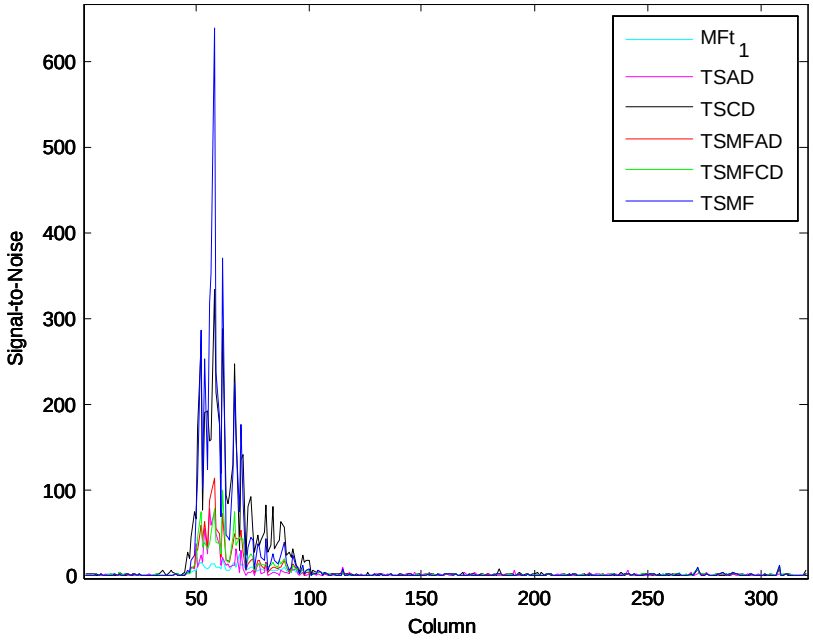

Figure 6. Performance of cascaded detectors on a release of SF_6 (Field Data).

CONCLUSIONS

This paper presented a set of temporal-spectral detectors for target detection in hyperspectral imagery. This set is not complete since the *TSAD* and *TSCD* detectors can be coupled with any standard detector. The advantage of the coupled detectors is that they combine temporal knowledge with spectral knowledge and only alarm to temporally anomalous signals which are a good match spectrally with the target vector. The significant increase in SNR from this approach allows the detection thresholds to be raised and the false alarm rate to be greatly reduced. The FIRST data experiments demonstrated the effectiveness of this approach.

REFERENCES

[1] Jeffrey Q. Chambers, Gregory P. Asner, Douglas C. Morton, Liana O. Anderson, Sassan S. Saatchi, Fernando D.B. Espírito-Santo, Michael Palace, Carlos Souza Jr., "Regional ecosystem structure and function: ecological insights from remote sensing of tropical forests," *Trends in Ecology & Evolution*, Volume 22, Issue 8, August 2007, Pages 414-423

[2] A. Ben-David, S.K. Holland, G.L. Laufer, and J.D. Baker, "Measurements of atmospheric brightness temperature fluctuations and their implications on passive remote sensing," *Optics Express*, vol. 13, no. 22, pp. 8781-8800, Oct. 2005.

[3] A. Ben-David, R.G. Vanderbeek, S.W. Gotoff, and F.M. Amico, "The effect of spectral time lag correlation and signal averaging on airborne CO_2 DIAL measurements," *Proc. SPIE*, 3127, pp.234-246, 1997.

[4] I.S. Reed and X. Yu, "Adaptive Multiple-Band CFAR Detection of an Optical Pattern with Unknown Spectral Distribution," *IEEE Trans. Acoust. Speech Signal Process.*, 38 (10), 1990, pp. 1760-1770.

[5] D. Manolakis, D. Marden, G.A. Shaw, “Hyperspectral image processing for automatic target detection applications,” *Lincoln Laboratory Journal*, vol. 14, no. 1, pp. 79-116, 2003.
[6] FIRST (Field-Portable Imaging Radiometric Spectrometer Technology) hyperspectral sensor manufactured by TELOPS (Quebec, Canada).